Microdomain Structure of an ABC-Type Triblock Polymer of Polystyrene–Poly[(4-vinylbenzyl)dimethylamine]–Polyisoprene Cast from Solutions

Mitsuhiro Shibayama, Hirokazu Hasegawa, Takeji Hashimoto,* and Hiromichi Kawai

Department of Polymer Chemistry, Faculty of Engineering, Kyoto University, Kyoto 606, Japan. *Received July 28, 1981*

ABSTRACT: A styrene–(4-vinylbenzyl)dimethylamine–isoprene ABC-type triblock polymer having a fairly narrow molecular weight distribution was synthesized by sequential anionic polymerization with *sec*-butyllithium as the initiator and benzene as the polymerization solvent. The morphology of characteristic microdomain structures which exist in solvent-cast films was studied by small-angle X-ray scattering (SAXS) and transmission electron microscope investigations and compared with the morphology of AB- and BC-type diblock polymers. The results are summarized as follows: (1) Each block chain segregates (phase separates) into respective microdomains, which results in the coexistence of three phases in the solid state. The three-phase structure was directly observed under transmission electron microscopy of ultrathin sections stained by osmium tetraoxide and phosphotungstic acid. (2) The size of each domain is of the order of the unperturbed chain dimension of the corresponding block chain, indicating that the domain morphology is typical of that formed by "microphase separation". (3) SAXS curves exhibit multiple-order Bragg reflections, clearly resolvable up to sixth-order scattering maxima, indicating that the bulk specimens have a three-phase microdomain structure with long-range periodic order, as observed under the electron microscope. (4) Some unique microdomain structures are observed for the triblock polymer, i.e., alternating lamellar domains of A- and B-block chains in which microdomains of C-block chains are dispersed in B lamellae in a regular two-dimensional array (see Figure 3a).

I. Introduction

The colloidal and morphological behaviors of block polymers composed of incompatible amorphous polymers have been extensively studied during the past decade. At present, morphology of the microdomain structures that are formed by the microphase separation of constituent block chains during solidification processes is well understood in terms of molecular parameters,[1-11] especially in the strong segregation limit, i.e., for the block-polymer systems having strong repulsive interaction between the constituent block chains. The sizes of the microdomain and domain-boundary thickness are quantitatively estimated as a function of molecular weights,[8,9] fractional compositions, temperature,[11] and amount of homopolymers solubilized;[10] some of these results have been quantitatively compared with statistical thermodynamic theories of the microdomains.[2-7] Fine agreement between the theoretical and experimental results has been obtained on the lamellar microdomains,[8] while some deviations have been found for the spherical microdomains and explained in terms of nonequilibrium and equilibrium aspects of the domain formation during the solidification process.[9]

The progress in the studies of microphase separation and microdomain morphology of AB- and ABA-type block polymers has naturally attracted attention to extending the studies not only for tapered block copolymers of two incompatible components to modify miscibility of unlike block chains for a given pair of components A and B[12-15] but also for a triblock composed of three incompatible components, i.e., ABC-type block polymers, with the expectation of novel colloidal and morphological behaviors in comparison with those of AB- and ABA-type block polymers.

The synthesis of the ABC-type triblock polymers began to appear in the literature in 1974, and almost ten different triblock polymers have been reported up to present. Most of them, however, are limited in their components, being composed commonly of polystyrene and polybutadiene (or polyisoprene) with another component for which a wide variety of polymers such as poly(α-methylstyrene),[16] poly(ethylene sulfide),[17] poly(2-vinylpyridine),[18,19] poly(*p*-*tert*-butylstyrene),[20] poly(ethylene oxide),[21] poly(4-vinylpyridine),[19,22,23] poly(methyl methacrylate),[24] and poly[(4-vinylbenzyl)dimethylamine][1] have been used. Despite numerous investigations of these triblock polymers, relatively few characteristics related to the ABC three-component molecular architecture have been found. This is partly due to difficulties in finding selective staining agents for distinguishing three-phase morphology by electron microscopy and partly due to difficulties in finding nonselective solvents for the three components. When selective solvents are used as the casting solvent, the volume occupied by the respective block chains in the solutions will change during solvent evaporation, which may result in morphological transitions among spherical, cylindrical, and lamellar microdomains. If the solvent evaporation rate is faster than or roughly equal to the relaxation rate of the morphological transition, an ill-defined nonequilibrium morphology becomes frozen-in at a certain concentration, prohibiting the system from achieving the equilibrium solid-state morphology.

In a previous paper of this series,[1] Matsushita et al. discussed anionic polymerizations of AB-, BC-, and ABC-type block polymers of styrene (S), (4-vinylbenzyl)dimethylamine (A), and isoprene (I), using *sec*-butyllithium as an initiator in benzene. A sequential order of SAI was found to give the most monodispersed triblock polymers with the least side reactions. The SAI triblock polymer films cast from dioxane solutions were found to have a three-phase microdomain structure (i.e., the respective block chains are segregated into the respective microdomains) by means of transmission electron microscopy on ultrathin sections stained by osmium tetraoxide (OsO_4) and phosphotungstic acid (PTA).

In this paper the morphological behavior of the same SAI triblock polymer as described above will be investigated in more detail as a function of casting solvents. The three-phase microdomain structures will be quantitatively examined by means of electron microscopy (section III-1) as well as small-angle X-ray scattering (SAXS) (sections III-2 and IV). The microdomain size will be contrasted qualitatively with that predicted from a microphase sep-

0024-9297/82/2215-0274$01.25/0

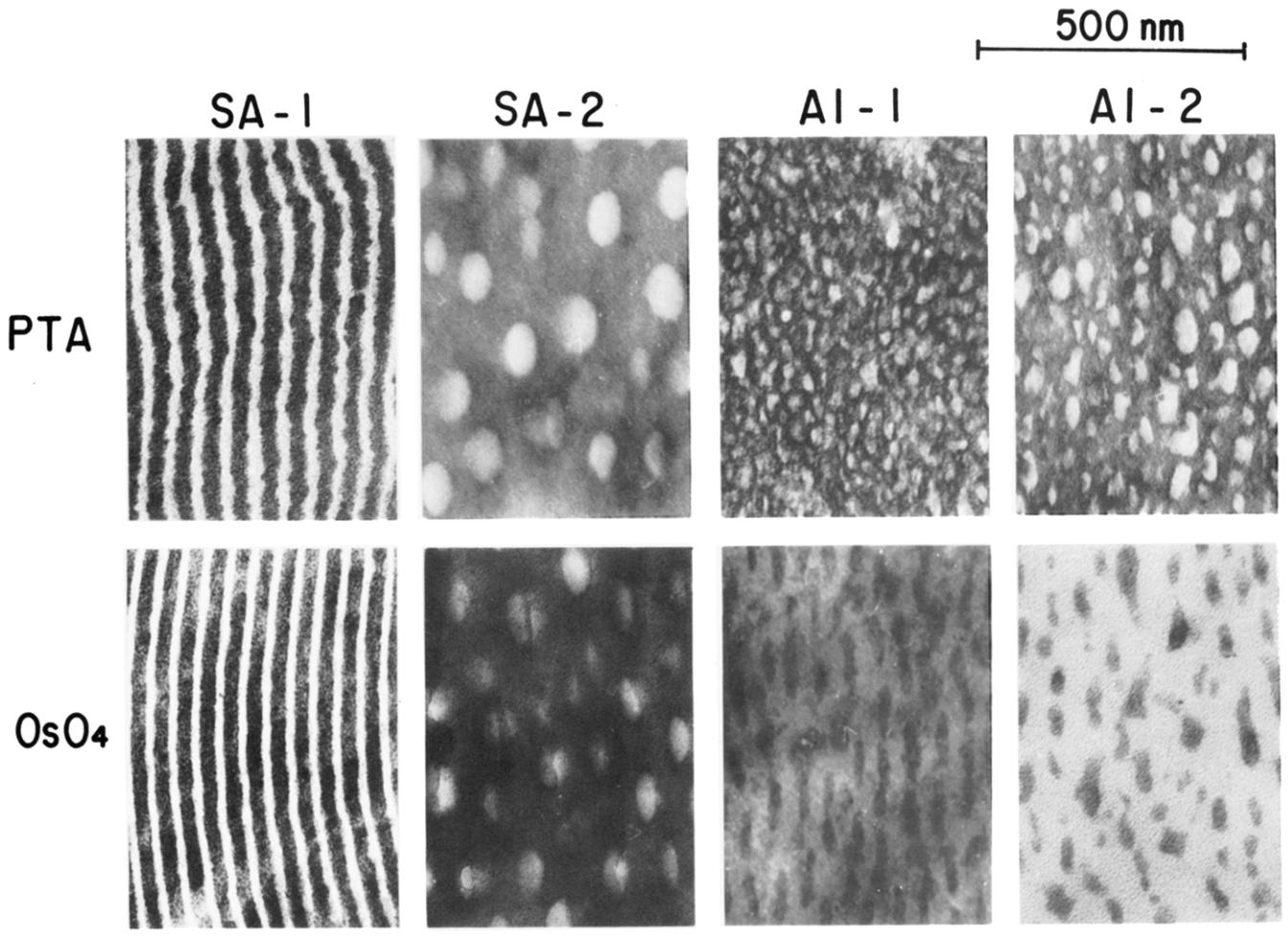

Figure 1. Transmission electron micrographs of ultrathin sections of the film specimens cast from dioxane solutions and stained by PTA (upper figures) and OsO_4 (bottom figures).

aration in strong segregation and incompressible limits (section V).

II. Test Specimens and Experimental Methods

The specimens used in this experiment were one triblock polymer of SAI, two diblock polymers of SA, and two diblock polymers of AI, which were designated as SAI-1, SA-1, SA-2, AI-1, and AI-2, respectively, in the previous paper.[1] Table I summarizes the characterizations of the block polymers. Each diblock polymer was cast from about 5% solutions of dioxane, while the triblock polymer was cast from about 5% benzene, tetrahydrofuran (THF), and dioxane solutions into thin films of about 100-μm thickness by evaporating the solvents gradually. The thin films were further dried under vacuum until they reached constant weight. The molecular weights and weight percent of polystyrene (S), poly[(4-vinylbenzyl)dimethylamine] (A), and polyisoprene (I) block chains were determined by measuring molecular weights of precursors which were sealed off before the second or third monomer was added. The weight fractions evaluated this way were in agreement with those estimated from elemental analyses.

Transmission electron microscopic observations were conducted with a JEM-100U microscope (Japan Electron Optics Laboratory Co. Ltd., Tokyo, Japan) operated at 80 kV on the ultrathin sections of the stained specimens. The objective aperture cutoff was at 0.014 $Å^{-1}$. OsO_4 and PTA were used as selective staining agents for the I and A components, respectively. The films were embedded in epoxy resin, trimmed, stained with aqueous solution of OsO_4 or PTA for 1 week, and then cut into ultrathin sections of several-hundred-angstrom thickness with an LKB ultratome Type 4801A (main unit) and 4802A (control unit). The microtomy was done at room temperature with a glass knife, and the thin sections were floated on a boat filled with water. The thickness of the sections was estimated from the interference color.

Table I
Characterization of Block Polymers

sample code[a]	$10^{-3}M_n$				wt %		
	S	A	I	total	S	A	I
SA-1	58	46		104	56	44	
SA-2	116	75		191	61	39	
AI-1		58	30	89		66	34
AI-2		126	98	224		56	44
SAI-1	60	64	40	164	37	39	24

[a] S, polystyrene; A, poly[(4-vinylbenzyl)dimethylamine]; I, polyisoprene.

The SAXS patterns were taken with a Huxley-Holmes point-focusing camera and with a Rigaku-Denki high-brilliancy rotating-anode Rotaflex RU-z X-ray generator as a microfocused X-ray source as described in our previous paper.[25] The SAXS intensity distributions were measured with a scintillation counter having a pulse height analyzer. Nickel-filtered Cu Kα radiation from a rotating-anode generator with a power of 40 kV and 200 mA was used as an incident beam. The beam was collimated by a four-slit system whose details are also described elsewhere.[26]

The observed scattering intensities were corrected for air-scattering and absorption and were normalized by sample thickness. The scattering curves that were taken with the incident beam normal to the film surface ("through" radiation) were also corrected for the slit-height smearing. The scattering curves that were taken with the incident beam parallel to the film surfaces ("edge" radiation) were not corrected for the slit-height smearing since the SAXS intensity was dependent on azimuthal angle. In most of the cases, however, the alternating lamellar structure is highly oriented with its interfaces parallel to the film surfaces, and moreover, the line-shaped image of the incident beam is set

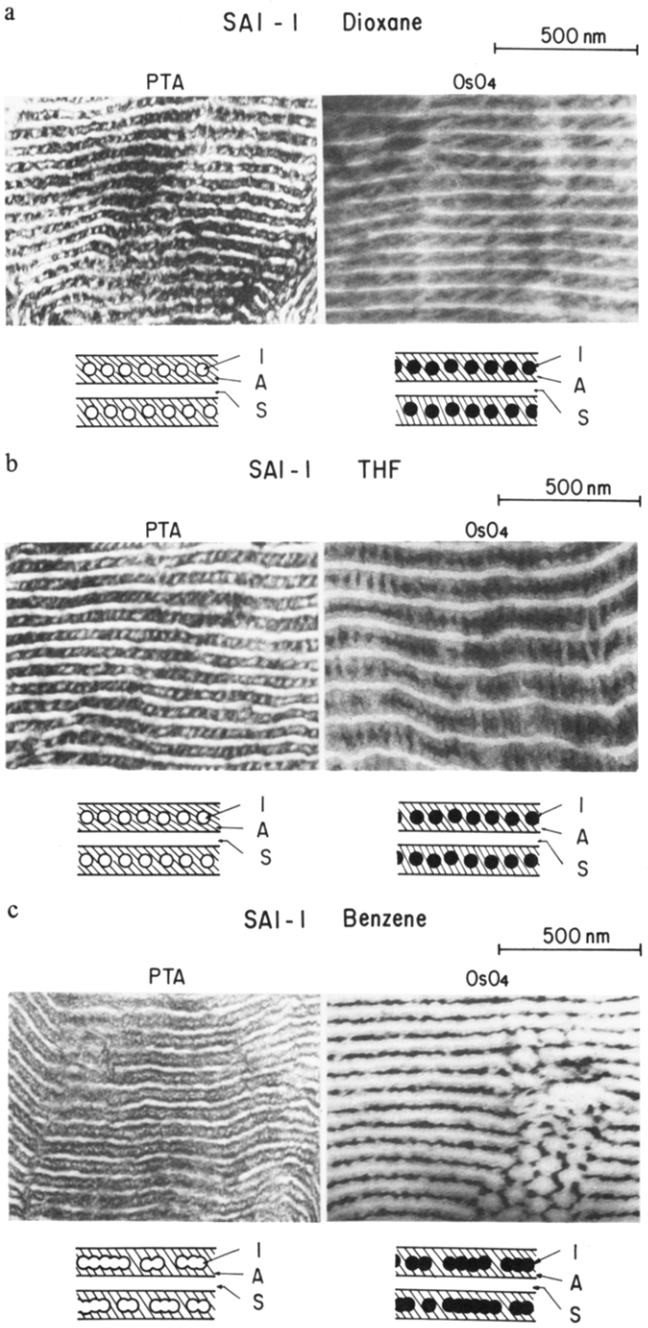

Figure 2. Transmission electron micrographs of ultrathin sections of the SAI-1 triblock polymers cast from (a) dioxane, (b) THF, and (c) benzene solutions and stained by PTA (left) and OsO_4 (right).

parallel to the surfaces so that the scattering curves measured in a direction perpendicular to the film surfaces are not significantly smeared by the slit-height smearing effect.

III. Results

1. Electron Microscopy. Figure 1 shows electron micrographs of a series of diblock polymers, all cast from dioxane solutions and stained with PTA (top figures) and OsO_4 (bottom figures). As can be seen in the micrographs of SA-1 and SA-2, both PTA and OsO_4 stain the domains composed of A chains, i.e., the dark and bright domains are those composed of A and S chains, respectively. On the other hand, as can be seen in the micrographs of AI-1 and AI-2 specimens, PTA and OsO_4 have a complementary effect on staining; i.e., they selectively stain the domains composed of A and I chains, respectively. AI-1 and AI-2 have microdomains of I chains dispersed in a matrix of A

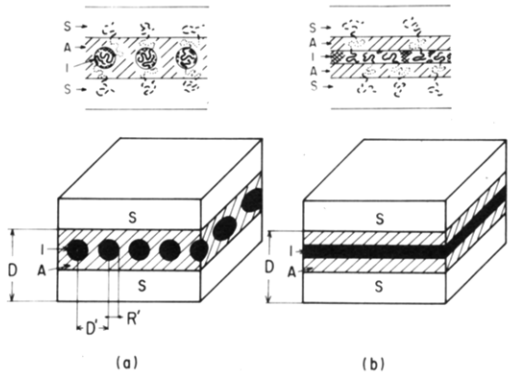

Figure 3. Schematic illustrations of the three-phase microdomain structures of the SAI-1 triblock polymers and their corresponding molecular packing.

chains. PTA does not stain the domains composed of I chains. OsO_4 stains both A and I domains with a different contrast; I domains are stained more heavily than A domains.

From the relationship between the morphology of the microdomains and the fractional composition of the diblock polymers,[27] SA-1 and AI-2 are expected to have alternating lamellar microdomains, while SA-2 and AI-1 are expected to have cylindrical microdomains, provided that the casting solvent is nonselective for the respective polymers. Some contradictions from the expected morphologies are seen in the micrographs, which are best understood in terms of selectivity of the solvent to the respective polymers; i.e., dioxane is a good solvent of A and a poor solvent of I. We assume here that the microdomain morphology developed in the concentrated solutions of the selective solvent tends to be fixed at certain concentration levels and results in a morphology in the solid state with further solvent evaporation.

Figure 2a–c shows the electron micrographs of the triblock polymer SAI-1 cast from dioxane, THF, and benzene, respectively. The left and right micrographs in each figure are obtained by staining with PTA and OsO_4, respectively. Figure 2 demonstrates, with good consistency with Figure 1, that PTA stains A domains only, whereas OsO_4 stains both A and I domains with a different contrast; I domains are stained more heavily than A domains.

Figure 2 indicates that SAI-1 has complicated mesomorphic structures in which I domains are dispersed in A lamellar domains. The A lamellae (containing I domains) and S lamellae are alternatively arranged in space and form a regular one-dimensional repetitive structure. Continuity of I domains in the A lamellae generally depends on casting solvent and casting condition, as seen in the figure. That is, for the particular film specimens cast from dioxane and THF, the isoprene domains are dispersed in the A lamellae as schematically illustrated in the bottom half of each figure. On the other hand, for the particular film specimens cast from benzene, the dispersed I domains tend to be interconnected to result in, more or less, a continuous isoprene domain as illustrated in the bottom half of Figure 2c.

Figure 3 illustrates a simplified version of typical morphologies as observed in this study: (a) spherical domains of I dispersed in a more or less regular two-dimensional array in A lamellae (a model for film specimens cast from dioxane and THF) and (b) an I lamella dispersed in an A lamella (a model for the benzene-cast films). The figure also represents a possible molecular packing of S, A, and I chains in the microphase-separated domain system. It should be noted, however, that the morphology of I do-

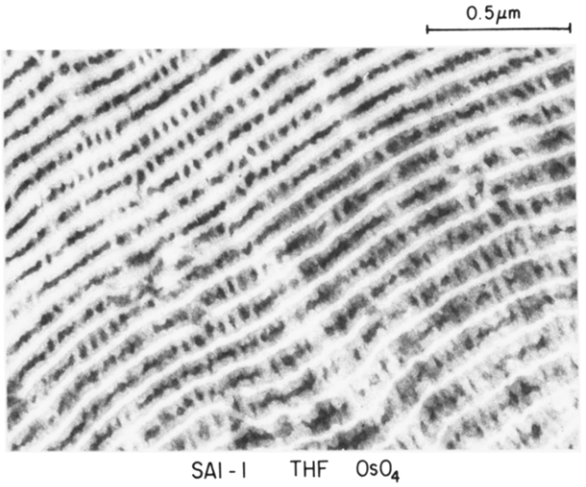

Figure 4. Electron micrograph showing coexistence of the three-phase microdomain structure of SAI-1 for the specimens cast from THF solutions and stained by OsO_4.

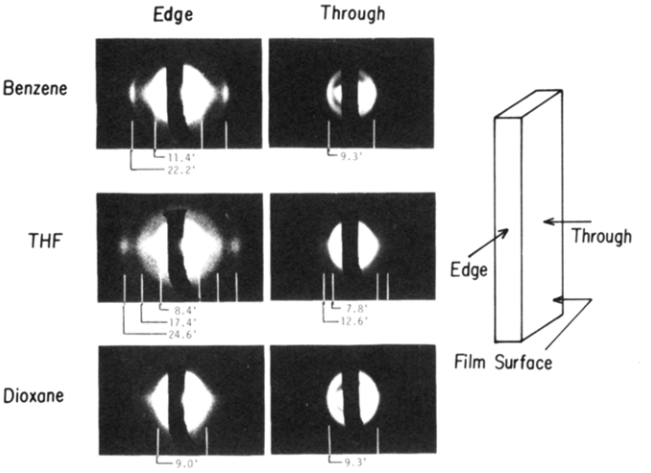

Figure 5. SAXS patterns taken with a point-focusing camera of the SAI-1 triblock polymer films cast from benzene, THF, and dioxane solutions.

mains may be affected by solvent evaporation rate (i.e., a kinetic factor) as well as by the solvent effect (i.e., a thermodynamic factor). Thus in order to understand the effect of casting solvents on the morphology of the triblock polymers, one must clarify the equilibrium and nonequilibrium aspects of the domain morphology. In this study the solvent evaporation rate was not carefully controlled.

Figure 4 shows more clearly coexistence of the three-phase microdomain structure of SAI-1 for the specimens cast from THF solution and stained by OsO_4. The lamellae, especially those in the right-bottom portion of the micrograph, appear as if their thicknesses vary gradually. This may be due to the fact that the wavy lamellae are cut obliquely to their normal. The detailed internal structure of the A lamellae can be more clearly resolved in that portion cut obliquely to the lamellar normals.

Each of the two types of morphology shown in Figure 3 is one of the unique morphologies for the ABC-type triblock polymer. The triple-layered morphology of –(SAIA)– in Figure 3b has already been found by Arai et al.[23] for an ABC-type triblock polymer of styrene, butadiene, and 4-vinylpyridine. A unique feature of the ABC-type block polymers is the strong constraint on the central B chains. That is, both ends of B must be anchored to A and C domains, which must affect strongly the swelling behavior, mechanical properties, and the power of the block polymers to solubilize[28] the B homopolymers.

2. SAXS Studies. Figure 5 shows SAXS patterns taken with the point-focusing camera of the edge- and through-radiation geometries of the SAI-1 film specimens cast from solutions of benzene, THF, and dioxane. The through-radiation patterns exhibit a single scattering maximum, with the exception of double maxima for the THF-cast films, with no azimuthal-angle dependence. On the other hand, the edge-radiation patterns exhibit more than three orders of maxima, with extremely high azimuthal-angle dependence. The scattered intensity is concentrated in a direction parallel to the film normals except for the specimens cast from dioxane solution, for which the pattern is almost the same as that for through-radiation.

The higher order scattering maxima for these specimens are attributed to a single long identity period of the lamellar-type microdomains as discussed in section III-1. For our film-preparation conditions the domains tend to orient themselves with their interfaces parallel to the film surfaces. The degree of planar orientation seems to depend

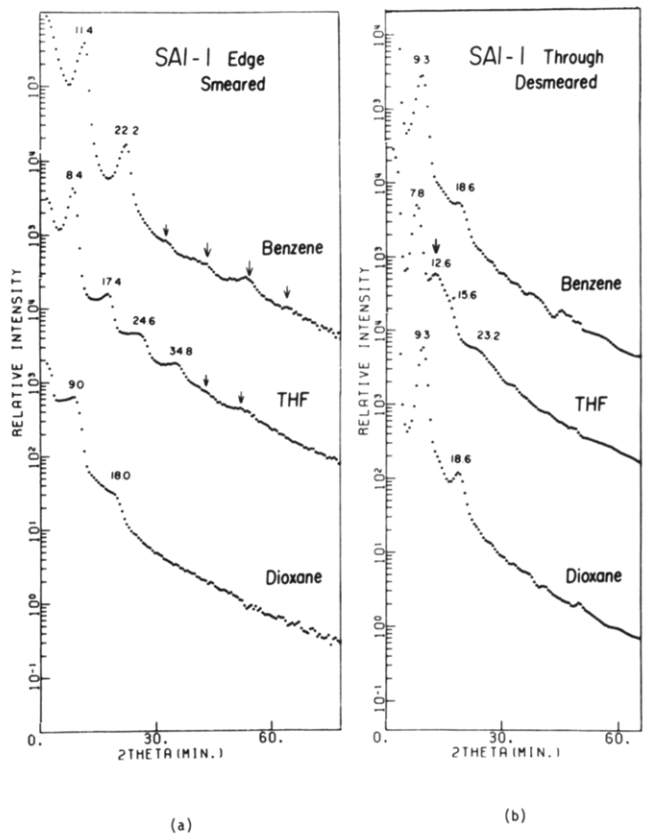

Figure 6. SAXS intensity distributions for the SAI-1 triblock polymer films cast from benzene, THF, and dioxane solutions: (a) edge radiated and smeared; (b) through radiated and desmeared.

on the solvent and the solvent evaporation rate. For the film specimens cast from dioxane solutions, the domain orientation was found to be almost random from the transmission electron microscopic observations.

Parts a and b of Figure 6 show, respectively, the photometrically measured SAXS intensity distributions for the respective specimens for the edge- and through-radiation geometries. The edge-radiation curves exhibit higher order scattering maxima up to the sixth-order, and for the benzene- and THF-cast films, all the maxima can be assigned to a single identity period of the regularly arranged lamellar type microdomains. The higher order scattering maxima indicate existence of long-range, regular spatial

Table II
Domain Properties of SAI-1 As Evaluated from Electron Microscopy (EM) and SAXS

cast solvent	D, nm			D', nm		R', nm	
	EM	SAXS edge	SAXS through	EM	SAXS	EM	SAXS
dioxane	57	58.8	56.9	30		13	—
THF	68	62.3	67.9	40	42.0	12	—
benzene	57	47.1	56.9				—

order of the microdomains.[8,29] The through radiation gives a few scattering maxima whose origins are roughly in agreement with those obtained from the edge radiation.

Close observation of Figure 6, however, reveals that the scattering curves obtained from edge radiation are different than those obtained from through radiation in following aspects: (1) The identity period measured from the edge-radiation curves is not identical with that measured from the through-radiation curves. This discrepancy must arise partly from the comparison between the smeared (edge) and desmeared (through) data and partly from the nature of the lamellar packing, i.e., the spacing is shorter for the domains with their lamellar normals oriented parallel to the film normal than for those with their normals oriented perpendicular to it when the lamellae are preferentially oriented. It should be noted that when one desmears the edge-radiation data of the dioxane-cast specimens which show isotropic scattering behavior, the scattering curve naturally becomes identical with the desmeared through-radiation data. (2) A scattering maximum at $2\theta = 12.6'$ (marked by an arrow) between the first- ($2\theta = 7.8'$) and second-order ($2\theta = 15.6'$) maxima from the long identity period, observed under through radiation for the films cast from THF solution, cannot be resolved in the scattering curve measured under edge radiation. This is an essential difference between the scattering curves measured under edge and through radiation. This extra maximum observed in the through-radiation data is best interpreted in terms of an interparticle interference between the spherical domains of I dispersed in a two-dimensional array within the matrix of A (i.e., reflecting spacing D' in Figure 3a). We were not able to determine the two-dimensional lattice structure since the higher order scattering maxima from the lattice were not resolvable. In the edge-radiation geometry this maximum attributed to the spacing D' should appear in the equatorial direction, i.e., in the direction perpendicular to the film normal, and therefore cannot be observed in the meridional scattering, i.e., the scattering along the film normals.

In the through-radiation scattering curves, this extra scattering maximum associated with the dispersed I domains is less distinct for the films cast from benzene than for the films cast from THF, indicating that the I domains tend to form a continuous phase (as found in Figure 2a for benzene-cast films). Table II summarizes the domain properties, D, D', and R' (defined in Figure 3) as evaluated from the SAXS results (Figure 6) and electron microscopic observations (Figure 2).

IV. Scattering from a Three-Phase System

We shall contrast here the scattering from a three-phase lamellar system composed of S, A, I, and A lamellae as a repeat unit (see Figure 3b for the simplified model of the microdomain structure observed in the benzene-cast films (Figure 2c)) with that from a two-phase alternating lamellar system, composed of S and I, for example. In order to facilitate the comparisons, we assume that both systems have a highly regular order as characterized by a one-dimensional macrolattice in the direction perpendicular to their interfaces (i.e., the x axis in Figure 7) and that the lamellae in the two systems are perfectly oriented, with their normals parallel to the x axis. In this case differences in the scattering behaviors of the two systems are attributed to the differences in the particle-scattering behaviors. Thus we consider below the particle scattering along the meridional direction, i.e., along the x-axis direction.

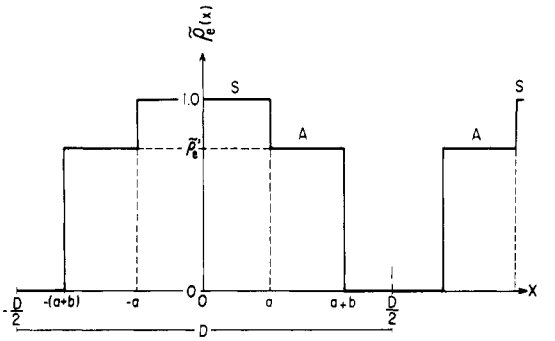

Figure 7. Relative electron density profile $\tilde{\rho}_e(x)$ across the interfaces of the (S–A–I–A) three-phase lamellar system. D is the identity period and a and b are associated with the thickness of S and A lamellae, respectively.

Table III
List of Physical Constants

physical constants	polymer S	polymer A	polymer I
mass density, ρ_K (g/cm^3)	1.052	1.013	0.925
electron density, ρ_{eK} (electrons/cm^3)	3.4×10^{23}	3.33×10^{23}	3.09×10^{23}
segment density, ρ_{oK} (mol/cm^3)	10.1×10^{-3}	6.28×10^{-3}	13.6×10^{-3}
Kuhn's segment length, b_K (nm)	0.68	0.68[a]	0.67
degree of polymerization, Z_K	576	397	587
molecular weight	6.0×10^4	6.4×10^4	4.0×10^4

[a] Assumed.

The relative electron density $\tilde{\rho}_e(x)$ of the particle in the three-phase lamellar system is given by, as in Figure 7

$$\begin{aligned} \tilde{\rho}_e(x) &= 1 \qquad \text{for } |x| \le a \\ \tilde{\rho}_e(x) &= \tilde{\rho}_e' \qquad \text{for } a < |x| \le a + b \\ \tilde{\rho}_e(x) &= 0 \qquad \text{for } |x| > a + b \end{aligned} \tag{1}$$

where

$$\tilde{\rho}_e' = \rho_{eA}/(\rho_{eA} - \rho_{eI}) \tag{2}$$

ρ_{eK} (K = A, S, or I) is the electron density of the K domain, which can be calculated from mass density ρ_K

$$\rho_{eK} = N_A \rho_K Z_{eK}/m_K \tag{3}$$

where N_A is Avogadro's number and Z_{eK} and m_K are, respectively, the number of electrons and the molecular weight of a monomeric unit of the K component (see Table III). The quantities a and b are associated with the thickness of the S and A lamellae, respectively, and are related to the volume fractions of S and A (defined as ϕ_S and ϕ_A, respectively) and the long identity period D

$$a = \phi_S D/2 \qquad b = \phi_A D/2 \tag{4}$$

The volume fraction of the I domains is then given by

$$\phi_I = 1 - \phi_S - \phi_A \tag{5}$$

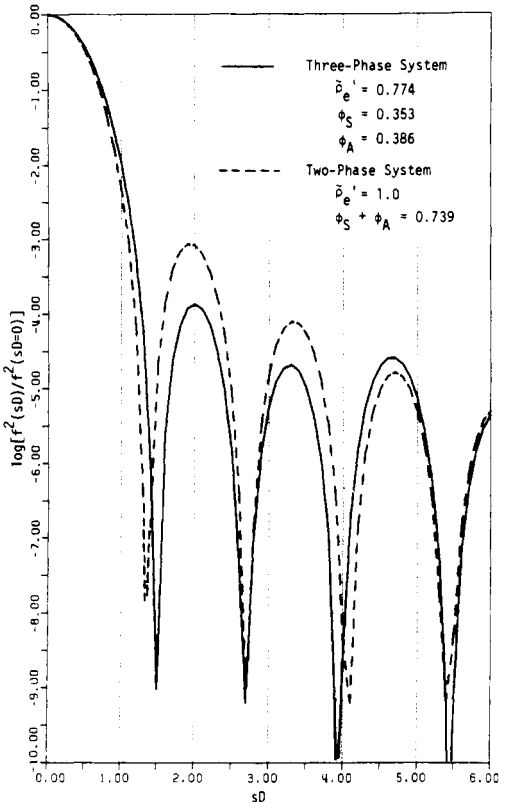

Figure 8. Relative particle scattering intensity distribution $f^2(sD)/f^2(sD = 0)$, with the reduced scattering angle sD for the three-phase system (solid line) with $\tilde{\rho}_e' = 0.774$, $\phi_S = 0.353$, and $\phi_A = 0.386$ and its limiting system (broken line) with $\tilde{\rho}_e' = 1$, $\phi_S + \phi_A = 0.739$, equivalent to a two-phase system composed of alternating S (or A) and I lamellae.

The scattering amplitude from the particle $f(s)$ is then given by

$$f(s) \sim \int \tilde{\rho}_e(x) \exp(-2\pi isx)\, dx \tag{6}$$

$$f(s) \sim (1/sD)\{(1 - \tilde{\rho}_e') \sin(2\pi\phi_S sD) + \tilde{\rho}_e' \sin[2\pi(\phi_S + \phi_A)sD]\} \tag{7}$$

where

$$s = (2 \sin\theta)/\lambda \tag{8}$$

λ is the X-ray wavelength, and 2θ is the scattering angle. By assuming ρ_K is equal to the mass density of pure K polymer, one can calculate $\tilde{\rho}_e$ from eq 2 and 3 and also ϕ_K from fractional composition of the SAI-1 specimens and from ρ_K. The ϕ_K values thus evaluated are 0.353, 0.386, and 0.261 for S, A, and I, respectively, and $\tilde{\rho}_e'$ is 0.774. Thus one can evaluate the particle scattering intensity for the three-phase system.

Figure 8 shows the relative scattered intensity distribution from the particle, $f^2(s)/f^2(s = 0)$, with the reduced scattering angle sD (D is the long identity period), for the three-phase system (solid line, $\tilde{\rho}_e' = 0.774$, $\phi_S = 0.353$, and $\phi_A = 0.386$) and its limiting system (broken line, $\tilde{\rho}_e' = 1$, $\phi_S + \phi_A = 0.739$), equivalent to a two-phase system composed of alternating S (or A) and I lamellar domains.

It should be noted that for a given specimen of SAI-1 triblock polymer, the particle scattering intensity distribution for the three-phase lamellar structure is almost identical with that for the two-phase lamellar structure, and thus the general features of the SAXS scattering curve (for the benzene-cast SAI-1 films in Figure 6a) are almost identical with those previously observed for the polystyrene–polyisoprene (SI) diblock polymers having alternating lamellar microdomain structure.[8,25,29] Thus the observed resemblance in the scattering behaviors between this particular three-phase system and the two-phase system for the SI diblock polymers is not surprising at all but quite predictable.

A slight difference in the scattering behaviors of the three-phase and two-phase systems exists in that the three-phase system shows a modulated damping of the peak height with sD, while the two-phase system shows a monotonous decrease of the peak height with sD. The particle scattering affects the entire scattering behavior. For example, the third and fourth scattering maxima from the benzene-cast films are very depressed compared with the fifth maxima, which may be explained in terms of relatively weak scattered intensity from the particle at sD = 3 and 4 (Figure 8).

V. Thermodynamic Analyses of Domain Properties

In section III the identity period D of the microdomain of SAI-1 triblock polymers was estimated to be 50–70 nm from EM (section III-1) and SAXS studies (section III-2). In this section we shall study whether the observed size of the domain is predictable from the molecular parameters of SAI-1 or pertinent to that formed as a consequence of microphase separation.

In view of the specific molecular packing of S-, A-, and I-block segments in the microdomain structure as shown in Figure 3, the domain identity period D should be of the order of the unperturbed chain dimension of the SAI-1 triblock polymer. The repulsive interactions between the constituent-block chains tend to expand the chain dimension, but we neglect this effect for a rough estimation. We assume

$$D \sim \langle R_0^2\rangle_S^{1/2} + \langle R_0^2\rangle_A^{1/2} + \langle R_0^2\rangle_I^{1/2} \tag{9}$$

where $\langle R_0^2\rangle_K^{1/2}$ (K = S, A, or I) is the unperturbed root mean square of the end-to-end vector of a K-block chain. For polystyrene $\langle R_0^2\rangle_S^{1/2} = 0.067 M_S^{1/2}$ nm, where M_S is molecular weight of S.[30] If we assume the same numerical constant 0.067 for other block chains, D is estimated to be 46.8 nm, which is in good agreement with the lower limit of the observed identity period.

We may be able to elaborate on our estimation of the domain identity period D one step further by using a hypothesis of "stepwise-microphase separation" and by applying the theories of microdomain structure of two-component systems as developed by Meier[2,3] and Helfand.[4-7] The hypothesis would state, for example, that microphase separation occurs between S and a homogeneous solution of A and I (a first-step microphase separation), which is followed by the second-step microphase separation between A- and I-block chains. The hypothesis may be reasonable in view of the lack of truly common solvents for the three polymers. We further assume that the alternating lamellar microdomain structure composed of S and a mixture of A and I is formed as a consequence of the first-step microphase separation and that the second-step microphase separation does not significantly change the identity period D of the lamellar microdomain formed by the first-step separation. Although the validity of this assumption in the specific scheme of the two-step separation (i.e., separation between S and the rest of the chains, followed by separation within the rest of the chains) requires future investigation, we may roughly estimate D based in this assumption. Then we can apply the theories developed by Meier and Helfand for the two-component systems.

We consider the AI-diblock chain as a single chain designated by R. The material R has an average segment

density ρ_{0R}, Kuhn segment length b_R, degree of polymerization Z_R, and interaction parameter χ against S

$$\rho_{0R} = (\rho_{0A}\rho_{0I})^{1/2} \quad (10)$$

$$\rho_{0R}b_R^2 = (1/2)\rho_{0A}b_A^2 + (1/2)\rho_{0I}b_I^2 \quad (11)$$

$$Z_R = \rho_{0R}[Z_A/\rho_{0A} + Z_I/\rho_{0I}] \quad (12)$$

$$\chi = 0.142 \quad (13)$$

where, as before, A and I stand for poly[(4-vinylbenzyl)-dimethylamine] and polyisoprene, respectively. The equations relating the molecular parameters in eq 10–13 to D were described in detail in our previous paper (eq 19 and 29[8]) and will not be repeated here. Table III summarizes the physical constants required for the calculation of D. The domain identity periods thus calculated from Meier's and Helfand's theories are identical with each other and equal to 74.4 nm, which agrees quite well with the upper limit of the observed domain identity period.

From the above discussion it is reasonable to assume that the domain structure as found in this study originates from pure microphase separation.

Acknowledgment. We acknowledge Professor M. Nagasawa and Y. Matsushita, Department of Synthetic Chemistry, Nagoya University, Nagoya, Japan, and Professor T. Fujimoto, Faculty of Engineering, Technological University of Nagaoka, Niigata, Japan, for kindly supplying the samples.

References and Notes

(1) Matsushita, Y.; Choshi, H.; Fujimoto, T.; Nagasawa, M. *Macromolecules* **1980**, *13*, 1053.
(2) Meier, D. J. *J. Polym. Sci., Part C* **1969**, *26*, 81.
(3) Meier, D. J. *Prepr., Polym. Colloq., Soc. Polym. Sci. Jpn., Kyoto* **1977**, 83.
(4) Helfand, E. *Macromolecules* **1975**, *8*, 552.
(5) Helfand, E.; Wasserman, Z. R. *Macromolecules* **1976**, *9*, 879.
(6) Helfand, E.; Wasserman, Z. R. *Macromolecules* **1978**, *11*, 960.
(7) Helfand, E.; Wasserman, Z. R. *Macromolecules* **1980**, *13*, 994.
(8) Hashimoto, T.; Shibayama, M.; Kawai, H. *Macromolecules* **1980**, *13*, 1237.
(9) Hashimoto, T.; Fujimura, M.; Kawai, H. *Macromolecules* **1980**, *13*, 1660.
(10) Hashimoto, H.; Fuiimura, M.; Hashimoto, T.; Kawai, H. *Macromolecules* **1981**, *14*, 844.
(11) Fujimura, M.; Hashimoto, H.; Kurahashi, K.; Hashimoto, T.; Kawai, H. *Macromolecules* **1981**, *14*, 1196.
(12) Zelinski, R.; Childers, C. W. *Rubber Chem. Technol.* **1968**, *41*, 161.
(13) Hsieh, H. L. In "Block and Graft Copolymers"; Burke, J. J., Weiss, V., Eds.; Syracuse University Press: Syracuse, N.Y., 1973.
(14) Aggarwal, S. L.; Livigni, R. A.; Marker, L. F.; Duclek, T. J. In ref 13.
(15) Tsukahara, Y.; Nakamura, N.; Hashimoto, T.; Kawai, H.; Nagaya, T.; Sugiura, Y.; Tsuge, S. *Polym. J.* **1980**, *12*, 455.
(16) Fielding-Russel, G. S.; Pillai, P. S. *Polymer* **1974**, *15*, 97.
(17) Cooper, W.; Hale, T.; Walker, J. S. *Polymer* **1974**, *15*, 175.
(18) Price, C.; Lally, T. P.; Stubbersfield, R. *Polymer* **1974**, *15*, 543.
(19) Luxton, A. R.; Quig, A.; Delvaux, M. J.; Fetters, L. J. *Polymer* **1978**, *19*, 1320.
(20) Fetters, L. J.; Firer, E. M.; Dafauti, M. *Macromolecules* **1977**, *10*, 1200.
(21) Koestier, D. W.; Bantjes, A.; Feijen, J.; Lyman, D. J. *J. Polym. Sci., Polym. Chem. Ed.* **1978**, *16*, 511.
(22) Arai, K.; Kotaka, T.; Kitano, Y.; Yoshimura, K. *Macromolecules* **1980**, *13*, 457.
(23) Arai, K.; Kotaka, T.; Kitano, Y.; Yoshimura, K. *Macromolecules* **1980**, *13*, 1670.
(24) Riess, G.; Schlienger, M.; Marti, S. *J. Macromol. Sci., Phys.* **1980**, *B17*, 355.
(25) Hashimoto, T.; Todo, A.; Itoi, H.; Kawai, H. *Macromolecules* **1977**, *10*, 377.
(26) Todo, A.; Hashimoto, T.; Kawai, H. *J. Appl. Crystallogr.* **1978**, *11*, 588.
(27) Inoue, T.; Soen, T.; Hashimoto, T.; Kawai, H. *J. Polym. Sci., Part A-2* **1969**, *7*, 1283.
(28) Inoue, T.; Soen, T.; Hashimoto, T.; Kawai, H. *Macromolecules* **1970**, *3*, 87.
(29) Hashimoto, T.; Todo, A.; Nagatoshi, K.; Hasegawa, H.; Kawai, H. *Macromolecules* **1974**, *7*, 364.
(30) Ballard, D. G. H.; Wignall, D. G.; Schelten, J. *Eur. Polym. J.* **1973**, *9*, 965.